The Functional Activity of the Human Serotonin 5-HT$_{1A}$ Receptor Is Controlled by Lipid Bilayer Composition

M. Gertrude Gutierrez,[1] Kylee S. Mansfield,[1] and Noah Malmstadt[1,*]
[1]Mork Family Department of Chemical Engineering and Materials Science, University of Southern California, Los Angeles, California

ABSTRACT   Although the properties of the cell plasma membrane lipid bilayer are broadly understood to affect integral membrane proteins, details of these interactions are poorly understood. This is particularly the case for the large family of G protein-coupled receptors (GPCRs). Here, we examine the lipid dependence of the human serotonin 5-HT$_{1A}$ receptor, a GPCR that is central to neuronal function. We incorporate the protein in synthetic bilayers of controlled composition together with a fluorescent reporting system that detects GPCR-catalyzed activation of G protein to measure receptor-catalyzed oligonucleotide exchange. Our results show that increased membrane order induced by sterols and sphingomyelin increases receptor-catalyzed oligonucleotide exchange. Increasing membrane elastic curvature stress also increases this exchange. These results reveal the broad dependence that the 5-HT$_{1A}$ receptor has on plasma membrane properties, demonstrating that membrane lipid composition is a biochemical control parameter and highlighting the possibility that compositional changes related to aging, diet, or disease could impact cell signaling functions.

INTRODUCTION

G protein-coupled receptors (GPCRs) account for 2% of the human genome; over 800 have been identified (1). They are the target of ~40% of pharmaceuticals on the market (2). GPCRs are integral membrane proteins with seven transmembrane α-helices. They associate with heterotrimeric G proteins on the cytosolic side of membranes. Upon binding an extracellular ligand, a GPCR can catalyze GDP/GTP exchange on the G protein alpha subunit, eliciting an intracellular signaling cascade resulting in events such as apoptosis or cell proliferation (3). GPCRs, upon binding ligands, undergo dynamic conformational changes in the transmembrane region, suggesting that properties of the surrounding lipid bilayer can alter the dynamics of receptor activation (4,5). The effects of bulk lipid bilayer properties on proteins have been demonstrated extensively for GPCR rhodopsin (6), indicating that membrane-protein interactions likely play a significant role in the function of other GPCRs.

Lipid compositional dependence of GPCRs is important because the composition of the plasma membrane varies with age, diet, and disease state, making lipid bilayer modulation of GPCR function a possible mode of disease etiology (7). Variation in plasma membrane composition across tissues may lead widely distributed GPCRs to behave differently in different tissue types (8).

Membrane lipid composition is known to affect the behavior of integral membrane proteins in general and GPCRs in particular (6,9–13). In reviews by Lee (2004) and Brown (1994 and 2012), the lipid compositional effects on proteins are conceptualized in terms of changes in bulk bilayer properties and chemically nonspecific interactions of bilayers and proteins (6,12,13). Changes in bulk bilayer material properties such as curvature stress and line tension due to membrane composition (experimentally testable via lipid substitutions) can shift the equilibrium between various protein conformations.

There has been extensive study of the effect of various lipid bilayer properties on the GPCR rhodopsin. Hydrophobic mismatch, bilayer-induced protein oligomerization, curvature elastic stress, lipid structure, lateral pressure profiles in lipid bilayers, and the effects of close range (annular) and long range (nonannular) lipids on rhodopsin have all been reported to shift the equilibrium between the inactive meta-I state (MI) and the active meta-II state (MII) (6,12–17). In particular, adding phosphoethanolamine lipids to lipid bilayers increases bilayer curvature stress, and shifts the rhodopsin equilibrium from MI toward MII (15,16,18). Cholesterol, which has membrane-ordering effects, shifts

the equilibrium toward MI (16,19,20). Rhodopsin activity also depends on bilayer thickness, increasing in bilayers that match the thickness of the protein transmembrane domain (21). Furthermore, rhodopsin-rhodopsin interactions at physiological lipid/protein ratios of 70:1 favor the MI inactive state due to oligomerization or superposition of lipid domains surrounding the GPCR (16).

Based on evolutionary relationships (80% of GPCRs are class A—or rhodopsin-like—receptors), there is reason to believe that other GPCRs may display similar dependencies (10,22,23). In addition, cholesterol binding may play a role in GPCR function. Hanson et al. reported a cholesterol binding site in the adenosine 2A (A_{2A}) receptor; they further identified 96 GPCRs with sequence homology to this binding site (24). Although these results suggest that GPCRs should in general be sensitive to lipid bilayer composition, current knowledge regarding the role that lipids play in the activity of GPCRs other than rhodopsin is scant.

An important rhodopsin-like GPCR is the human serotonin 5-HT$_{1A}$ receptor (5-HT$_{1A}$R), which is involved in a number of psychological and stress-related diseases (2). Chattopadhyay and co-workers (25) have extensively studied the cholesterol dependence of 5-HT$_{1A}$R. Working largely with systems based on depletion and replenishment of membrane components in ligand-binding and cell-based activity assays, they have shown that cholesterol depletion can inhibit downstream receptor activity of 5-HT$_{1A}$R (26–28). However, they have also reported that depending on the cell type, depletion of the membrane ordering components cholesterol and sphingomyelin can either increase or decrease agonist binding of 5-HT$_{1A}$R (29–32). Membrane lipid composition clearly affects the function of 5-HT$_{1A}$R, though with conflicting results largely depending on cell type, it is essential to have a protein reconstitution system in which the lipid environment can be stringently controlled.

Here, we measure the lipid-dependent activity of 5-HT$_{1A}$R by reconstituting the protein in giant unilamellar protein-vesicles (GUPs) with controlled composition using an agarose hydration method (Fig. 1). We previously used this method to characterize 5-HT$_{1A}$R cosegregation with the liquid disordered phase in liquid-liquid phase separating membranes (33). For this work, we encapsulate BODIPY-GTPγS, a quenched fluorophore, into GUPs with reconstituted 5-HT$_{1A}$R and cognizant G protein subunits. Incubating GUPs with an extracellular agonist, 8-hydroxy-2-(dipropylamino)tetralin hydrobromide (8-OH-DPAT), triggers receptor activation and exchange of G protein-bound-GDP for BODIPY-GTPγS. This irreversible exchange unquenches BODIPY-GTPγS fluorescence (Fig. 1; Movie S1 in the Supporting Material). Receptor-catalyzed oligonucleotide exchange can therefore be measured as a change in fluorescence intensity. We use this system to study the effects of lipid order, cholesterol concentration, and membrane curvature stress on 5-HT$_{1A}$R activity. We observe that increasing the concentration of membrane-ordering
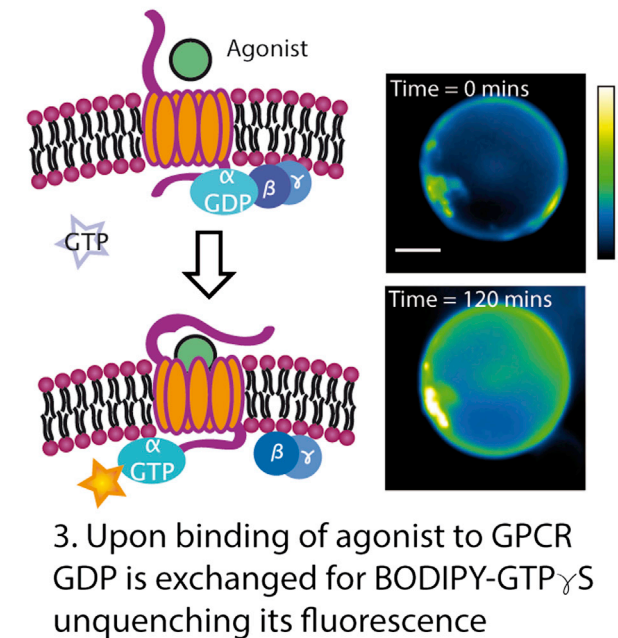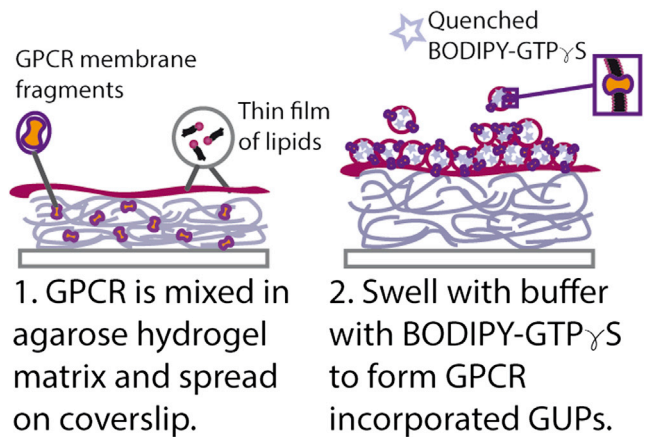

FIGURE 1 Schematic of protein functionality assay. GUPs are formed via hydrogel rehydration. Incubation with agonist unquenches encapsulated BODIPY-GTPγS fluorescence via G protein binding. Fluorescence is tracked over time (see *inset micrographs*). To see this figure in color, go online.

components increases 5-HT$_{1A}$R-catalyzed oligonucleotide exchange, and adding cholesterol analogs that have a greater tendency to order the membrane than cholesterol itself results in greater increases in receptor activity. Introduction of curvature stress from lipids that prefer nonlamellar phases also affects the 5-HT$_{1A}$R activity as is the case for rhodopsin.

MATERIALS AND METHODS

Materials

1-palmitoyl-2-oleoyl-*sn*-glycero-3-phosphocholine (POPC), brain sphingomyelin, (BSM), cholesterol (Chol), and 1,2-dioleoyl-*sn*-glycero-3-phosphoethanolamine (DOPE) were acquired from Avanti Polar Lipids (Alabaster, AL)

(USA). The fluorescently tagged lipid ATTO-488-DPPE and ATTO-550-DPPE were obtained from ATTO-TEC (Siegen, Germany). Ergosterol was from Sigma Aldrich (St. Louis, MO) and epicholesterol was from Steraloids (Newport, RI). Membrane fragments containing 5-HT$_{1A}$R were from Perkin Elmer (Waltham, MA), the monoclonal antibody to 5-HT$_{1A}$R was from EMD Millipore (Billerica, MA), and G$_{\alpha i}$ antibodies were from Thermo Fisher (Waltham, MA). The agonist 8-Hydroxy-2-(dipropylamino)tetralin hydrobromide (8-OH-DPAT) was from Sigma Aldrich. The antagonist spiperone was from Tocris (Avonmouth, UK). Solutions of ligands were made to 10 mM in dimethyl sulfoxide (DMSO), except for 8-OH-DPAT, which was prepared at 10 mM in 200 mM sucrose in phosphate buffered saline (PBS) (pH 7.4). BODIPY-GTPγS and QSY7 were obtained from Life Technologies (Waltham, MA). Other chemicals including low melting temperature agarose, PBS, methanol (MeOH), DMSO, diphenylhexatriene (DPH), chloroform (CHCl$_3$), sucrose, and glucose were of analytical grade (Sigma Aldrich). All chemicals and biomolecules were used as shipped without further purification. Sykes-Moore chambers (Bellco, Vineland, NJ), standard 25 mm no. 1 glass coverslips (ChemGlass, Vineland, NJ), and flat bottom 96-well plates (BD Biosciences, San Jose, CA) were used throughout all experiments. 18.2 MΩ cm Milli-Q water was used in all experiments (EMD Millipore). Protein desalting microspin columns and NHS-Rhodamine (both from Thermo Fisher) were used as per manufacturer's instructions.

Fabrication of vesicles and protein incorporation

25 mm-diameter no. 1 circular coverslips were cleaned via sonication in methanol for 30 min at 35°C. Coverslips were dried and plasma treated in a PDC-32G benchtop plasma cleaner (Harrick Plasma, Ithaca, NY) for 15 min. Coverslips were held in Sykes-Moore chambers for vesicle formation.

Protein-incorporated GUPs were formed using methods previously published (25). Briefly, a lipid film was made on freshly cleaned coverslips from lipid solutions of 3–4 mg/mL in CHCl$_3$. Solvent was evaporated using a stream of N$_2$ gas. A 1:1 v/v mixture of membrane fragment suspension and agarose (3% w/v) was drop casted onto the same coverslip and a thin film was formed. Protein concentration was estimated based on the reported protein concentrations as supplied in the membrane fragments. Protein was added to the GUP formation system to achieve a final receptor concentration of 0.2 nM in the GUP suspension. This corresponds to a synthetic lipid/added-protein ratio of 100:1 and lipid/receptor ratio of 2×10^6:1. For control giant unilamellar vesicle (GUV) fabrication, protein was omitted from the hydrogel film and only 1.5% w/v agarose was used. The film was allowed to gel and the system was hydrated with 200 mM sucrose in PBS (pH 7.4) with 100 μM spiperone and BODIPY-γ-FL-GTP (5 μM). Lipid films were swollen for 30 min above the transition temperature of the lipids, ~40°C. Vesicles were harvested from the coverslip by gentle pipetting and diluted in 3$\times$ of an iso-osmotic glucose solution (200 mM glucose in PBS, pH 7.4). GUPs were allowed to sediment in glucose for 30 min at room temperature.

Liposomes for encapsulation in quenching assay controls were made by extruding agarose-formed giant vesicles. GUVs were made of POPC with 0.2 mol % ATTO-550-DPPE fluorescent lipid and protein omitted from the agarose film. After swelling the vesicles were harvested and extruded through a 400 nm filter with 12 passes.

Liposomes used for anisotropy measurements were made via sonication. Investigated compositions were doped with 0.5 mol % DPH. 1 mg/mL of the lipid solution was dried to form a film on the side of a cell culture tube and rehydrated with water. Lipids were then sonicated for 1 h at 37°C.

5-HT$_{1A}$ activity assay

GUPs without any dye-labeled lipids were prepared and settled and transferred to a flat bottom 96-well plate. 8-OH-DPAT was added to each well to a final concentration of 150 nM immediately before reading fluorescence. Control GUPs were run without the addition of the agonist. As additional controls for the system, rehydration buffer with BODIPY-GTPγS, rehydra-

tion buffer with BODIPY-GTPγS and agonist, and protein in membrane fragments as shipped diluted in rehydration buffer with BODIPY-GTPγS and agonist were read. Protein in membrane fragments as shipped indicated the intrinsic receptor-catalyzed oligonucleotide exchange of the membrane preparations with their native lipid composition. Buffer with and without agonist were used for fluorescence correction (i.e., photobleaching or auto-fluoresence). Samples were read at physiological temperature 37°C every 5 min for 12 h to ensure complete activity assessment. Fluorescence reading of BODIPY-GTPγS unquenching was done on a BioTek Synergy H4 Microplate Reader (Winooski, VT) equipped with a xenon flash lamp. Excitation was set to 485/20 nm and emission at 528/20 nm at a read height of 7 mm.

Antibody labeling

5-HT$_{1A}$R monoclonal and G$_{\alpha i}$ antibodies were equilibrated to room temperature and conjugated to the NHS ester of rhodamine in DMSO at 10$\times$ molar excess. Sodium bicarbonate was added as per manufacturer's instructions to raise the solution pH to 8.0. The solution was allowed to react for 1 h at room temperature and overnight at 5°C. Rhodamine-labeled antibodies were subsequently desalted using spin columns according to the manufacturer's instructions. Labeled antibody ultraviolet-visible absorbance was read on a NanoDrop ND-1000 (Thermo Fisher). Rhodamine-labeled G$_{\alpha i}$ protein antibody concentration was determined to be 22 μM and labeling efficiency was calculated to be 1.15. Rhodamine-labeled 5-HT$_{1A}$ monoclonal antibody concentration was 3.2 μM with 1.41 labeling efficiency.

Antibody label fluorescence quenching to determine protein orientation

5-HT$_{1A}$R membrane fragments were incubated with rhodamine-labeled 5-HT$_{1A}$R monoclonal antibodies or rhodamine-labeled G$_{\alpha i}$ monoclonal antibodies, 1:1000 dilutions. The labeled protein mixture was included in the agarose film used for GUP formation. GUVs without protein for control and GUPs made of 0:3:2 and 1:0:0 POPC/BSM/Chol were fabricated as described previously. These GUVs and GUPs were prepared without any dye-labeled lipids. GUVs were incubated with rhodamine-labeled antibodies to demonstrate antibody specificity (Fig. S1). Vesicles were harvested, settled, and placed in observation chambers. Vesicles were imaged via epifluorescence before quenching. QSY7, a quenching molecule, was then added to the observation chambers at 0.1 μM final concentration and incubated in the dark for 10 min. GUPs were imaged after incubation and the amount of quenched fluorescence intensity was analyzed. GUVs without protein and with 0.2 mol % ATTO-488-DPPE were fabricated and settled and then incubated with QSY7 as control samples.

Fluorescence anisotropy measurements

Bilayer membranes were formed as liposomes. 1 mg of the desired lipid composition was dried as a thin film in a cell culture tube, rehydrated with Milli Q water, and sonicated as described previously. All lipid compositions were doped with 0.5 mol % DPH for membrane fluidity measurements via fluorescence anisotropy. Fluorescence anisotropy measurements were made at 37°C on a QuantaMaster 4 spectroflourometer equipped with a xenon arc lamp (75 W). Readings were performed using a slit width of 10 nm, excitation at 354 nm, and emission at 435 nm. All anisotropy readings were done for 60 s. Data from three separate samples were averaged and are presented.

Microscopy

Imaging was done on a TI-Eclipse inverted microscope (Nikon, Melville, NY) equipped with a spinning-disc CSUX confocal head (Yokogawa,

Tokyo, Japan) and a 16-bit Cascade II 512 electron-multiplied charge-coupled device camera (Photometrics, Huntington Beach, CA). Confocal excitation of fluorophores was done using 50 mW solid-state lasers at 491 nm for BODIPY-GTPγS and ATTO-488-DPPE (emission filter centered at 525 nm), and 561 nm for rhodamine (emission filter centered at 595 nm, all lasers from Coherent, Santa Clara, CA). All confocal images were taken using a Plan-Apo 60$\times$ NA1.43 oil immersion Nikon objective. Z-stack images were separated by 0.2 μm steps. Epifluorescence imaging was performed on the same microscope with illumination from a 130 W mercury lamp (Intensilight, Nikon). Rhodamine and ATTO-550-DPPE emission was excited using a green filter (528–552 nm bandpass, 540 nm cut-on wavelength). Temperature control during imaging was performed using a heating-cooling stage with a stability and accuracy of 0.1°C (Bioscience Tools, San Diego, CA).

Image processing

All images were processed and analyzed using ImageJ. All confocal images are presented as standard deviation projections of Z-stacks and were produced using standard ImageJ Stack Tools. Particle analysis and measurements were performed using ImageJ Analyze Tools. Fluorescent micrographs of vesicles using 491 nm excitation are shown using the ImageJ green lookup table, and micrographs using 561 nm excitation are shown using the Image J orange lookup table. All images are presented without any further processing adjustments or corrections and are scaled from minimum to maximum intensity.

Data analysis

Fluorescence microtiter results were collected and analyzed using JMP (SAS Institute, Cary, NC). About five separate GUP sample preparations were averaged to obtain a single curve for each of the compositions investigated. Standard error of the mean values for each data point were determined and are plotted as shaded areas around the curves showing the average values. Control curves are the average of all individual observations in a composition set (ternary POPC/BSM/Chol, binary POPC/Chol, binary POPC/DOPE, etc.). They include samples representing all the permutations of lipid ratios investigated. Upon obtaining the raw fluorescence intensities (au), they were converted to percent fluorescence intensity increase to account for variation in sample preparation. Furthermore, these were normalized to 1 to aid in comparing the rates of specific data sets. The data from each lipid composition were fit to a single exponential using the JMP mechanistic growth analysis and the rates were obtained. Statistical analysis using analysis of variance (ANOVA) followed by post-hoc Tukey Kramer pairwise comparison of means were done using JMP with a 95% confidence interval ($\alpha = 0.05$).

Fluorescence intensity analysis of GUPs before and after quenching was performed in ImageJ. A line segment was drawn across a GUP and the intensity profiles across GUP diameter were obtained (Fig. S2). Intensities across the same line segment of unquenched and quenched GUPs were averaged and the percent of retained fluorescence intensity was calculated.

RESULTS AND DISCUSSION

Protein orientation of GPCR 5-HT$_{1A}$ in GUPs

Protein orientation was determined in GUPs without dye-labeled lipids formed in the presence of rhodamine-labeled monoclonal antibody for either receptor (5-HT$_{1A}$R antibody) or G protein (G$_{\alpha i}$ antibody). The 5-HT$_{1A}$R antibody binds specifically to the cytosolic domain. A fluorescence quencher (QSY7) was added to the solution of GUPs. No GUP compositions investigated displayed microscale phase

separation or domain formation. QSY7 is a commercially available molecule that efficiently quenches the emission from a broad range of fluorophores via Förster resonance energy transfer and contact quenching (34). This charged, hydrophilic quencher accesses fluorophores only on GUP exteriors and does not cross the bilayer membrane (Fig. S3). GUPs made of 100% POPC and 60%:40% BSM/Chol (0% POPC) were formed in the presence of labeled antibodies and exposed to QSY7 (0.1 mg/mL final concentration) for 10 min at room temperature. Antibodies did not display nonspecific interactions with the bilayer membrane (Figs. S1 and S2). Fig. 2 A shows that in both lipid compositions, fluorescent labels on 5-HT$_{1A}$R antibodies retained over 90% of their initial intensity. This indicates that the reconstituted receptor was incorporated in a biased and correct orientation, with the cytoplasmic domain in the GUP interior. An ANOVA on these compositions did not yield a significant variation among conditions, F(2, 22) = 0.91, p > 0.35. A post hoc Tukey-Kramer analysis of mean pairs of the two GUP compositions ($\alpha = 0.05$) further rejected the null hypothesis that the means of the two
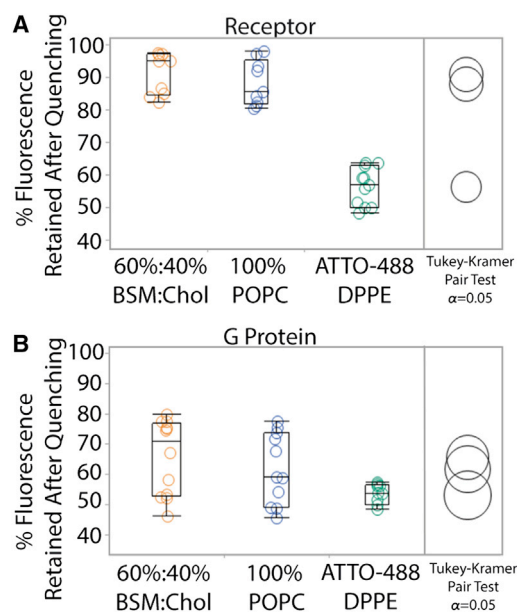

FIGURE 2 GPCR orientation determination. 100% POPC and 60%:40% BSM/Chol GUPs were formed with labeled antibodies to either the cytoplasmic domain of the GPCR or the G$_\alpha$ protein subunit. (A) Quenching of the fluorescent antibody bound to the cytoplasmic domain of 5-HT$_{1A}$R resulted in retention of ~90% of fluorescence. This indicates that receptors were oriented with the N-terminus extracellular and C-terminus interior. ANOVA indicated no significant difference between the two GUP samples, F(1, 22) = 0.91, p > 0.35, as also confirmed with post-hoc Tukey-Kramer analysis. (B) G proteins tagged with rhodamine-labeled antibody showed an unbiased distribution between the inner and outer bilayer leaflets with fluorescence intensity retention ~65%. There was no significant difference between the different GUP compositions, F(1,24) = 0.26 p > 0.61. Control GUVs without protein and labeled with fluorescent lipid, ATTO-488-DPPE, showed 50% fluorescent intensity retention after incubation with QSY7. To see this figure in color, go online.

GUP compositions are statistically different. The control for the data set was GUVs without protein formed with a fluorescently labeled lipid, ATTO-488-1,2-dihexadecanoyl-*sn*-glycero-3-phosphoethanolamine (ATTO-488-DPPE) and included at 0.2 mol %. The fluorescent label was quenched on the exterior of the GUV but retained on the interior (~50% intensity retention, see Fig. 2).

A similar analysis was done with rhodamine-labeled antibodies that bind to the $G_{\alpha i}$ subunit that couples to 5-HT$_{1A}$R (see Fig. 2 *B*). In this case, only ~65% of the original intensity remained after quenching with QSY7. Thus, G protein subunits did not display a significant bias to either the interior or exterior leaflet of our GUP bilayers. These measurements did not statistically differ between the lipid compositions, 100% POPC and 0% POPC (see Fig. 2 *B*).

The orientation of the receptor may be induced by membrane curvature (35). In forming GUPs using our method, GUPs initially form as small vesicles, likely of nanometer scale (Movie S2). Over time, these smaller vesicles coalesce to form giant unilamellar vesicles (Fig. S4) (36). At small vesicle diameters, membrane curvature is high, facilitating curvature-induced orientation. The retention of protein orientation in a biased and correct manner as facilitated by our method of GUP formation offers a platform that decreases the effects of incorrect receptor orientation in GPCR investigations. The lack of preference toward bilayer leaflets observed for the G proteins can be attributed to the fact that G proteins are anchored to the bilayer via palmitoylated lipid tails rather than being integral to the membrane.

Effects of lipid order on receptor-catalyzed oligonucleotide exchange

The effects of lipid order on 5-HT$_{1A}$R function were investigated by varying ternary compositions of GUPs made from POPC, BSM, and Chol. These GUPs were made without any fluorescently labeled lipids. None of the compositions investigated were liquid-liquid phase separating lipid mixtures (37). Compositions studied span from pure POPC (less ordered) to binary BSM/Chol (more ordered). Protein was added to the GUP formation system to achieve a final receptor concentration of 0.2 nM in the GUP suspension. This corresponds to a synthetic lipid/added-protein ratio of 100:1 and a lipid/receptor ratio of 2×10^6:1. GUPs are expected to contain ~20% of other lipid and other proteins contributed from membrane fragment preparations. The same product lot and concentration of membrane fragment preparation were used throughout all experiments, meaning that the lipid and other protein composition in GUPs from the membrane fragments remained a constant background composition. The composition-dependent effects observed in this report can therefore be attributed to the synthetic lipids used in our GUP preparations. 5-HT$_{1A}$R GUPs were fabricated in the presence of the antagonist spiperone to limit basal activity. GUPs were then exposed to excess
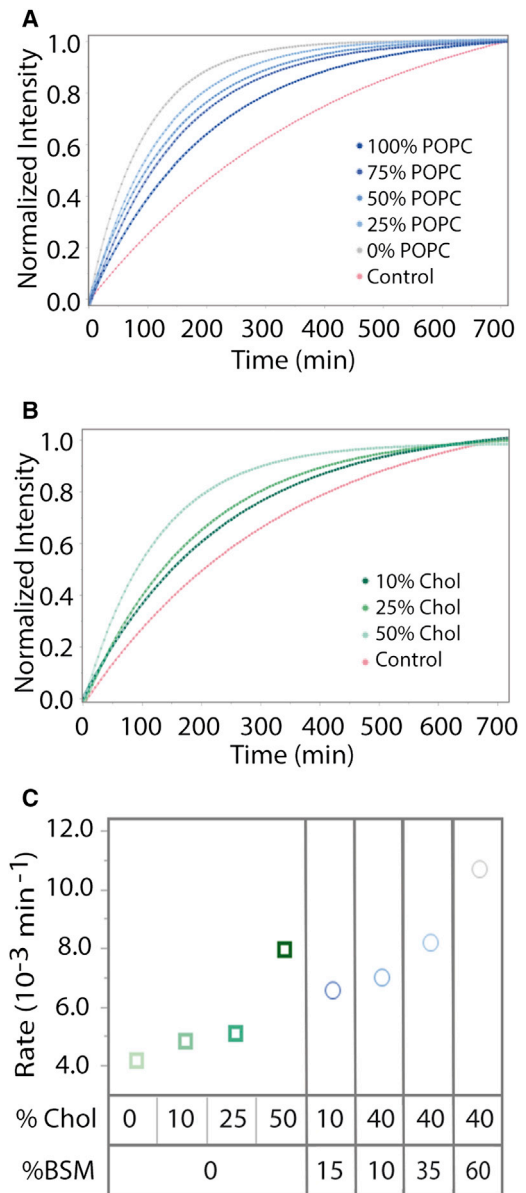

FIGURE 3 Receptor-catalyzed oligonucleotide exchange rates in ternary and binary GUPs. Each individual curve represents fluorescence intensity over time as an average of five observations with identical experimental conditions. The shaded area around the points indicates the standard error of the mean of the averaged samples. Control samples are the average of all observations of the listed compositions of GUPs tracked in the absence of agonist and are indicated in pink. (*A*) GPCR activity rate in GUPs with increasing amounts of ordering components, BSM and Chol, in ternary GUPs of POPC/BSM/Chol. Going from 100% POPC to 60%:40% BSM/Chol (0% POPC) shows an increased rate of receptor-catalyzed oligonucleotide exchange. (*B*) GPCR activity rate in binary GUPs of POPC/Chol. Increasing the amount of Chol in these systems increases the rate of receptor-catalyzed oligonucleotide exchange. (*C*) Plot of rates from (*A*) and (*B*) by Chol and BSM composition. Error bars are not included because they are smaller than the markers. See Table 1 for error data. Ternary GUPs indicated by circles in blue show faster rates than binary GUPs indicted by squares in green. To see this figure in color, go online.

agonist, 8-OH-DPAT, to determine rates of receptor-catalyzed oligonucleotide exchange (Fig. 1, *step 3*; evaluation of activity assay can be found in the Supporting Material, Figs. S5–S7, and Table S1). For functional assays, nonphase-separating GUPs were fabricated and transferred to 96-well plates and fluorescence measurements were taken every 5 min for 12 h (Fig. 3). Raw fluorescence intensity data were converted to percentages to account for differences in GUP sample size and then normalized to facilitate rate comparisons. Each fluorescence curve represents on average five separate GUP samples (Table 1). Percent intensity increase of each sample at each time point was averaged for the indicated composition. Control curves are averaged from all samples of a composition set without agonist, and represent basal activity (Fig. S8). Individual rates of control GUPs and GUPs exposed to agonist can be seen in Table 1. As seen in Fig. 3, increasing membrane-ordering components (BSM/Chol) increased the measured rate of receptor-catalyzed oligonucleotide exchange. Protein in membrane fragments as shipped was diluted in 200 mM sucrose in $1\times$ PBS with BODIPY-GTPγS, exposed to 8-OH-DPAT, and assayed using the same approach as the GUPs as a positive control for intrinsic activity; these were not preexposed to spiperone and displayed a rate of 5.29 ($\times 10^{-3}$) min^{-1}. GUPs made completely out of BSM/Chol had a rate constant over double that of pure POPC GUPs (10.83 vs. 4.26 ($\times 10^{-3}$) min^{-1}). Thus, it is observed that increasing the concentrations of the ordering components BSM and Chol increases 5-HT$_{1A}$R activity in our GUPs.

Previous work by the Chattopadhyay group has shown that ligand binding of 5-HT$_{1A}$R depends on cholesterol and sphingomyelin. They reported that cleaving the headgroup of sphingomyelin decreases the receptor's ligand binding ability (29). Furthermore, they reported that in solubilized membranes, depletion of cholesterol decreases ligand binding ability, whereas depletion of cholesterol in neuronal cells enhances ligand binding (31,32). These reports provide conflicting conclusions regarding the ligand binding ability of 5-HT$_{1A}$R, and further work on membrane ordering components on 5-HT$_{1A}$R and other GPCRs is relatively limited. Our results provide further insight into understanding the role of bulk bilayer membrane properties on GPCR activity, specifically the rates of receptor-catalyzed oligonucleotide exchange. Given that many GPCRs are thought to bind cholesterol (24); however, it is important to distinguish receptor modulation due to changes in bulk membrane properties from receptor modulation due to direct cholesterol binding.

Effects of cholesterol and cholesterol analogs on receptor-catalyzed oligonucleotide exchange

The direct effects of Chol associations with 5-HT$_{1A}$R on receptor functionality were investigated using binary POPC/Chol systems without fluorescently labeled lipids

TABLE 1 Summary of Rates from All Compositions

POPC	BSM	Chol	Agonist Rate (10^{-3} min^{-1})	Std. Error (10^{-3} min^{-1})	Control Rate (10^{-3} min^{-1})	Std. Error (10^{-3} min^{-1})
100	0	0	4.26	0.09	1.23	0.05
75	15	10	6.66	0.12	2.23	0.05
50	10	40	7.06	0.13	2.67	0.05
25	35	40	8.29	0.15	2.91	0.05
0	60	40	10.83	0.26	3.24	0.05
POPC		Chol				
90		10	4.91	0.11	1.97	0.10
75		25	5.18	0.15	2.94	0.05
50		50	8.06	0.22	3.09	0.05
POPC		Ergosterol				
90		10	10.19	0.15	3.59	0.07
75		25	12.82	0.23	3.88	0.06
50		50	17.26	0.34	6.22	0.87
POPC		Epicholesterol				
90		10	8.04	0.10	3.11	0.03
75		25	8.92	0.11	3.17	0.02
50		50	9.88	0.14	3.21	0.02
POPC		DOPE				
97.5		2.5	11.99	0.06	3.05	0.07
92.5		7.5	22.67	0.14	4.92	0.08
90		10	19.66	0.03	4.91	0.09
75		25	16.12	0.02	4.86	0.10
50		50	9.38	0.01	4.79	0.09

Lipid concentrations are given in mol %. Std., standard.

(Fig. 3, *B* and *C*; Table 1). At Chol concentrations of 0%, 10%, 25%, and 50%, we observed increasing rates of 5-HT$_{1A}$R catalyzed oligonucleotide exchange. The rates, as fitted from a single exponential curve, are shown in Table 1. The fluorescence intensity curves are depicted in Fig. 3 *B*. While increasing Chol concentration increased catalyzed exchange rates, GUPs with both ordering components Chol and BSM had a higher rate than any binary POPC/Chol GUP.

5-HT$_{1A}$R Chol dependence has been previously observed (32,38), but it is unclear whether the effects are due to direct cholesterol binding to the receptor or due to cholesterol-induced changes in bulk membrane bilayer properties (5,39). Such properties may include ordering, or the capacity of cholesterol to sequester ligands near the bilayer surface (40). Cholesterol has been shown to increase bilayer thickness and to alter the energy of membrane elastic deformations due to increased lateral area compressibility coefficient and elastic bending modulus (41). To determine if the effects of Chol are due to direct binding or changes in membrane properties (ordering, packing density, etc.), the effects of the Chol analogs epicholesterol and ergosterol were examined. Ergosterol is the primary sterol in fungal membranes and epicholesterol is a Chol diastereomer (42); their structures are shown in Fig. 4. The effects of ergosterol and epicholesterol are shown in Fig. 4, *A* and *B*. As the amount of either sterol increases, the measured rate of receptor-catalyzed oligonucleotide exchange increases. This suggests that changes in membrane properties rather than direct Chol binding result in increased receptor activity. A previous report suggested cholesterol binding increases the ligand binding ability of 5-HT$_{1A}$R but does not report on receptor-catalyzed oligonucleotide exchange of the serotonin receptor (27); thus, our results provide initial insight into the effects of cholesterol and its analogs on receptor-catalyzed exchange rates.

Our results further show that ergosterol has a greater effect than epicholesterol in increasing rates of oligonucleotide exchange. Ergosterol is known to induce more membrane ordering than epicholesterol or Chol, which is consistent with our results in the previous section (42). We performed fluorescence anisotropy measurements of vesicles formed without protein and doped with 0.5 mol % DPH to determine the relative degrees of ordering in bilayers of varying composition (43). Results shown in Table 2 indicate that lipid order increases from Chol to epicholesterol to ergosterol. The idea that membrane order is the key determinant of 5-HT$_{1A}$R activity is borne out by the fact that the most highly ordered compositions studied here (incorporating both Chol and BSM) (44) display the highest rates of receptor-catalyzed oligonucleotide exchange.

Effects of elastic curvature stress on receptor-catalyzed activity

Elastic curvature stress resulting from nonlamellar lipids in bilayer membranes has been shown to affect the MI-MII
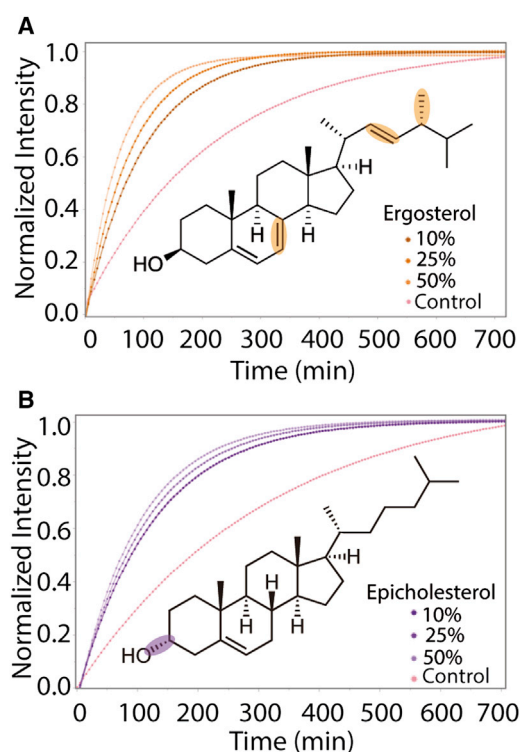

FIGURE 4 Receptor-catalyzed oligonucleotide exchange rate of GUPs made with Chol analogs. (*A*) Binary POPC/Ergosterol GUPs were assessed for receptor-catalyzed oligonucleotide exchange activity. As concentration of ergosterol was increased, exchange rate also increased. The chemical structure of ergostolerol is placed within the plot with its differences from Chol highlighted. (*B*) Binary POPC/Epicholesterol GUPs also showed an increase in receptor-catalyzed exchange rate with increasing amounts of epicholesterol. Epicholesterol is a diastereomer of Chol with the hydroxyl group on the alpha face of Chol, as shown in the chemical structure within the plot. Control curves are the average of all individual observations for the listed compositions of GUPs without agonist incubation. To see this figure in color, go online.

equilibrium of rhodopsin shifting it toward the MII state (17). To elucidate if elastic curvature stress as a membrane property affects 5-HT$_{1A}$R activity, GUPs made from POPC and DOPE were assessed. POPC/DOPE GUPs with 2.5%, 7%, 10%, 25%, and 50% DOPE (Figs. 5 and S9) and without fluorescently labeled lipids were analyzed. We observed that adding DOPE increased the measured GPCR activity rate overall; however, the rate initially increased then decreased with increasing DOPE going from 11.99 to 22.67 to 9.38 ($\times 10^{-3}$) min^{-1} (Table 1). The fastest rates measured in this system were faster than rates observed in all DOPE-free compositions reported; the slowest rates rivaled the fastest rates measured elsewhere. According to fluorescence anisotropy measurements (Table 2) POPC/DOPE GUPs are no more ordered than pure POPC membranes, thus the effects of DOPE are likely not due to membrane ordering as seems to be the case for Chol and the cholesterol analogs studied here.

The increased rate of 5-HT$_{1A}$R activity can be considered in terms of elastic curvature stress and bilayer membrane

TABLE 2   Bilayer Ordering Results as Determined by Fluorescence Anisotropy Measurements for All Lipid Compositions

% POPC	POPC/Chol/BSM (Anisotropy ± Std Dev)	POPC/Chol (Anisotropy ± Std Dev)	POPC/Ergosterol (Anisotropy ± Std Dev)	POPC/Epicholesterol (Anisotropy ± Std Dev)	POPC:DOPE (Anisotropy ± Std Dev)
100	0.146 ± 0.008				
90		0.168 ± 0.004	0.182 ± 0.003	0.171 ± 0.002	0.149 ± 0.003
75	0.184 ± 0.005	0.224 ± 0.001	0.215 ± 0.003	0.212 ± 0.004	0.143 ± 0.004
50	0.287 ± 0.012	0.248 ± 0.001	0.268 ± 0.002	0.241 ± 0.003	0.142 ± 0.001
25	0.271 ± 0.005				
0	0.331 ± 0.006				

Lipid concentrations are given in mol %. Std Dev, standard deviation.

pressure profile. Pure DOPE is known to exist in the curved hexagonal phase (H_{II}) at physiological temperatures (12). In compositions with at least 20% lamellar forming lipids, however, bilayers are formed with DOPE; these show increased membrane frustration due to negative curvature induced by the cone shape of DOPE. Coupling of the spontaneous curvature of phosphoethanolamine lipids lipid bilayers to the conformational changes of transmembrane proteins has also been suggested to relieve membrane stress, lowering the free energy of the system (12,13,15). As an annular lipid immediately next to the protein, DOPE can fill free volume between integral proteins and bilayer components; it can also assist in the hydrophobic matching of the lipid bilayer to the transmembrane domain of the protein (12). Lipids with negative curvature, such as DOPE, can deform to accommodate the hydrophobic length of the protein (10,12,15). Thus, the presence of DOPE in our GUPs with a lipid/protein ratio of 100:1, and a peak rate of 5-HT$_{1A}$R activity at 7.5–10 mol % DOPE could be explained in terms of the release of elastic curvature stress due to favorable lipid and protein interactions.

Membrane curvature has been linked to membrane pressure profiles in molecular dynamics simulations of bilayer membranes (45). Thus, the effects of DOPE on the GPCR may also be considered in terms of its modulation of the bilayer membrane pressure profile. In molecular dynamics studies, simulated DOPE pressure profiles show an additional negative peak as compared to DOPC (45). This negative peak is in the headgroup region of the membrane and is indicative of where the bilayer would contract to minimize free energy due to the cone shape of DOPE (45). Because the DOPE headgroup is small it changes membrane pressure and hydration, which may result in the modulation of GPCR function that we report here. Simulations with ergosterol in bilayer membranes also display a change in membrane pressure profiles similar to that seen with DOPE (46). Thus, the shape of DOPE lipids and the propensity for ergosterol to order lipids have similar effects on altering the membrane pressure profile; the mechanism by which this change affects protein function would therefore be common to both compositional changes.

CONCLUSIONS

We report direct observations showing lipid compositional dependence of 5-HT$_{1A}$R activity in GUPs. Increasing the concentration of order-inducing lipid components (Chol, ergosterol, epicholesterol, and BSM) increases the 5-HT$_{1A}$R-catalyzed oligonucleotide exchange rate of associated G proteins. Furthermore, we see significant rate increases in the presence of DOPE, suggesting that the elastic energy dependence widely reported for rhodopsin also holds true for 5-HT$_{1A}$R. Changes in membrane pressure profile due to DOPE and ergosterol may also modulate 5-HT$_{1A}$R function. Protein incorporation into model membranes using this approach allows for controlled compositional changes in protein membrane environment and the ease of the experimental method provides opportunities for evaluating the effects of various ligands and effectors on orphan GPCRs and other proteins. Stringent control of lipid composition in model membranes may further elucidate novel therapeutic approaches for diseases related to GPCR activity. This approach, therefore, provides a platform for evaluating lipidic parameters affecting GPCR activity that cannot be investigated using in vivo or traditional methods.
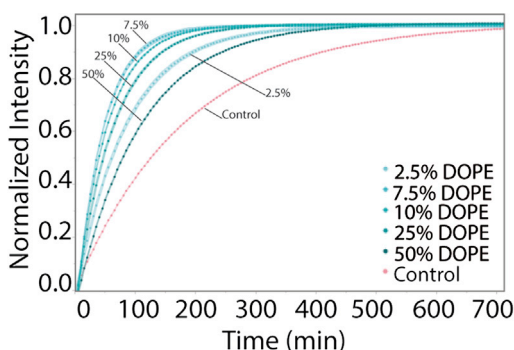

FIGURE 5   5-HT$_{1A}$ receptor-catalyzed oligonucleotide exchange rate of GUPs made of POPC/DOPE. The overall rates are well above other compositions investigated, ranging from 9.38 to 22.67 ($\times 10^{-3}$) min^{-1}, see Table 1. However, as DOPE mol % increases beyond 7.5% the protein functional rate decreases. To see this figure in color, go online.

SUPPORTING MATERIAL

AUTHOR CONTRIBUTIONS

ACKNOWLEDGMENTS

REFERENCES

1. Drews, J. 2000. Drug discovery: a historical perspective. *Science.* 287:1960–1964.

2. Xu, Y., J. Yan, …, Q. Wang. 2012. Neurotransmitter receptors and cognitive dysfunction in Alzheimer's disease and Parkinson's disease. *Prog. Neurobiol.* 97:1–13.

3. Kroeze, W. K., D. J. Sheffler, and B. L. Roth. 2003. G-protein-coupled receptors at a glance. *J. Cell Sci.* 116:4867–4869.

4. Kobilka, B. K. 2007. G protein coupled receptor structure and activation. *Biochim. Biophys. Acta.* 1768:794–807.

5. Chattopadhyay, A. 2014. GPCRs: lipid-dependent membrane receptors that act as drug targets. *Adv. Bio. P.* 2014:1–12.

6. Brown, M. F. 1994. Modulation of rhodopsin function by properties of the membrane bilayer. *Chem. Phys. Lipids.* 73:159–180.

7. Nicolson, G. L., and M. E. Ash. 2014. Lipid Replacement Therapy: a natural medicine approach to replacing damaged lipids in cellular membranes and organelles and restoring function. *Biochim. Biophys. Acta.* 1838:1657–1679.

8. Jain, M., S. Ngoy, …, R. Nilsson. 2014. A systematic survey of lipids across mouse tissues. *Am. J. Physiol. Endocrinol. Metab.* 306:E854–E868.

9. Escribá, P. V. 2006. Membrane-lipid therapy: a new approach in molecular medicine. *Trends Mol. Med.* 12:34–43.

10. Soubias, O., W. E. Teague, …, K. Gawrisch. 2014. The role of membrane curvature elastic stress for function of rhodopsin-like G protein-coupled receptors. *Biochimie.* 107 (Pt A):28–32.

11. Niu, S. L., D. C. Mitchell, and B. J. Litman. 2001. Optimization of receptor-G protein coupling by bilayer lipid composition II: formation of metarhodopsin II-transducin complex. *J. Biol. Chem.* 276:42807–42811.

12. Lee, A. G. 2004. How lipids affect the activities of integral membrane proteins. *Biochim. Biophys. Acta.* 1666:62–87.

13. Brown, M. F. 2012. Curvature forces in membrane lipid-protein interactions. *Biochemistry.* 51:9782–9795.

14. Botelho, A. V., T. Huber, …, M. F. Brown. 2006. Curvature and hydrophobic forces drive oligomerization and modulate activity of rhodopsin in membranes. *Biophys. J.* 91:4464–4477.

15. Botelho, A. V., N. J. Gibson, …, M. F. Brown. 2002. Conformational energetics of rhodopsin modulated by nonlamellar-forming lipids. *Biochemistry.* 41:6354–6368.

16. Soubias, O., and K. Gawrisch. 2012. The role of the lipid matrix for structure and function of the GPCR rhodopsin. *Biochim. Biophys. Acta.* 1818:234–240.

17. Soubias, O., W. E. Teague, Jr., …, K. Gawrisch. 2010. Contribution of membrane elastic energy to rhodopsin function. *Biophys. J.* 99:817–824.

18. Teague, W. E., Jr., O. Soubias, …, K. Gawrisch. 2013. Elastic properties of polyunsaturated phosphatidylethanolamines influence rhodopsin function. *Faraday Discuss.* 161:383–395, discussion 419–459.

19. Mitchell, D. C., M. Straume, …, B. J. Litman. 1990. Modulation of metarhodopsin formation by cholesterol-induced ordering of bilayer lipids. *Biochemistry.* 29:9143–9149.

20. Niu, S. L., D. C. Mitchell, and B. J. Litman. 2002. Manipulation of cholesterol levels in rod disk membranes by methyl-beta-cyclodextrin: effects on receptor activation. *J. Biol. Chem.* 277:20139–20145.

21. Soubias, O., W. E. Teague, Jr., …, K. Gawrisch. 2015. Rhodopsin/lipid hydrophobic matching-rhodopsin oligomerization and function. *Biophys. J.* 108:1125–1132.

22. Lebon, G., T. Warne, …, C. G. Tate. 2011. Agonist-bound adenosine A2A receptor structures reveal common features of GPCR activation. *Nature.* 474:521–525.

23. Rasmussen, S. G., H. J. Choi, …, B. K. Kobilka. 2007. Crystal structure of the human beta2 adrenergic G-protein-coupled receptor. *Nature.* 450:383–387.

24. Hanson, M. A., V. Cherezov, …, R. C. Stevens. 2008. A specific cholesterol binding site is established by the 2.8 A structure of the human beta2-adrenergic receptor. *Structure.* 16:897–905.

25. Jafurulla, M., and A. Chattopadhyay. 2013. Membrane lipids in the function of serotonin and adrenergic receptors. *Curr. Med. Chem.* 20:47–55.

26. Paila, Y. D., T. J. Pucadyil, and A. Chattopadhyay. 2005. The cholesterol-complexing agent digitonin modulates ligand binding of the bovine hippocampal serotonin 1A receptor. *Mol. Membr. Biol.* 22:241–249.

27. Jafurulla, M., B. D. Rao, …, A. Chattopadhyay. 2014. Stereospecific requirement of cholesterol in the function of the serotonin1A receptor. *Biochim. Biophys. Acta.* 1838 (1 Pt B):158–163.

28. Sengupta, D., and A. Chattopadhyay. 2012. Identification of cholesterol binding sites in the serotonin1A receptor. *J. Phys. Chem. B.* 116:12991–12996.

29. Jafurulla, M., T. J. Pucadyil, and A. Chattopadhyay. 2008. Effect of sphingomyelinase treatment on ligand binding activity of human serotonin1A receptors. *Biochim. Biophys. Acta. (Biomembranes).* 1778:2022–2025.

30. Singh, P., and A. Chattopadhyay. 2012. Removal of sphingomyelin headgroup inhibits the ligand binding function of hippocampal serotonin1A receptors. *Biochem. Biophys. Res. Commun.* 419:321–325.

31. Prasad, R., Y. D. Paila, …, A. Chattopadhyay. 2009. Membrane cholesterol depletion from live cells enhances the function of human serotonin(1A) receptors. *Biochem. Biophys. Res. Commun.* 389:333–337.

32. Prasad, R., Y. D. Paila, and A. Chattopadhyay. 2009. Membrane cholesterol depletion enhances ligand binding function of human serotonin1A receptors in neuronal cells. *Biochem. Biophys. Res. Commun.* 390:93–96.

33. Gutierrez, M. G., and N. Malmstadt. 2014. Human serotonin receptor 5-HT$_{(1A)}$ preferentially segregates to the liquid disordered phase in synthetic lipid bilayers. *J. Am. Chem. Soc.* 136:13530–13533.

34. Marras, S. A. E., F. R. Kramer, and S. Tyagi. 2002. Efficiencies of fluorescence resonance energy transfer and contact-mediated quenching in oligonucleotide probes. *Nucleic Acids Res.* 30:e122.

35. Bordignon, E. 2012. Site-directed spin labeling of membrane proteins. *Top. Curr. Chem.* 321:121–157.

36. Horger, K. S., D. J. Estes, …, M. Mayer. 2009. Films of agarose enable rapid formation of giant liposomes in solutions of physiologic ionic strength. *J. Am. Chem. Soc.* 131:1810–1819.

37. Veatch, S. L., and S. L. Keller. 2005. Miscibility phase diagrams of giant vesicles containing sphingomyelin. *Phys. Rev. Lett.* 94:148101–148104.

38. Shrivastava, S., T. J. Pucadyil, …, A. Chattopadhyay. 2010. Chronic cholesterol depletion using statin impairs the function and dynamics of human serotonin(1A) receptors. *Biochemistry.* 49:5426–5435.

39. Saxena, R., and A. Chattopadhyay. 2012. Membrane cholesterol stabilizes the human serotonin(1A) receptor. *Biochim. Biophys. Acta.* 1818:2936–2942.

40. Lopez, J. J., and M. Lorch. 2008. Location and orientation of serotonin receptor 1a agonists in model and complex lipid membranes. *J. Biol. Chem.* 283:7813–7822.

41. Needham, D., T. J. McIntosh, and E. Evans. 1988. Thermomechanical and transition properties of dimyristoylphosphatidylcholine/cholesterol bilayers. *Biochemistry.* 27:4668–4673.

42. Róg, T., M. Pasenkiewicz-Gierula, …, M. Karttunen. 2009. Ordering effects of cholesterol and its analogues. *Biochim. Biophys. Acta.* 1788:97–121.

43. Jähnig, F. 1979. Structural order of lipids and proteins in membranes: evaluation of fluorescence anisotropy data. *Proc. Natl. Acad. Sci. USA.* 76:6361–6365.

44. Björkbom, A., T. Róg, …, J. P. Slotte. 2010. Effect of sphingomyelin headgroup size on molecular properties and interactions with cholesterol. *Biophys. J.* 99:3300–3308.

45. Sodt, A. J., and R. W. Pastor. 2013. Bending free energy from simulation: correspondence of planar and inverse hexagonal lipid phases. *Biophys. J.* 104:2202–2211.

46. Vanegas, J. M., M. L. Longo, and R. Faller. 2011. Crystalline, ordered and disordered lipid membranes: convergence of stress profiles due to ergosterol. *J. Am. Chem. Soc.* 133:3720–3723.